Physica B 443 (2014) 24–34

Contents lists available at ScienceDirect

Physica B

journal homepage: www.elsevier.com/locate/physb

Electronic and optical properties of the SiB_2O_4 (B=Mg, Zn, and Cd) spinel oxides: An ab initio study with the Tran–Blaha-modified Becke–Johnson density functional

D. Allali [a], A. Bouhemadou [a,*], E. Muhammad Abud Al Safi [b], S. Bin-Omran [b,c], M. Chegaar [d], R. Khenata [e], A.H. Reshak [f,g]

[a] Laboratory for Developing New Materials and their Characterization, University of Setif 1, 19000 Setif, Algeria
[b] Department of Physics and Astronomy, College of Science, King Saud University, P.O. Box 2455, Riyadh 11451, Saudi Arabia
[c] Department of Physics, Faculty of Science & Humanitarian Studies, Salman Bin Abdalaziz University, Alkharj 11942, Saudi Arabia
[d] Department of Physics, Faculty of Science, University of Setif 1, 19000 Setif, Algeria
[e] Laboratoire de Physique Quantique et de Modélisation Mathématique (LPQ3M), Département de Technologie, Université de Mascara, 29000 Mascara, Algeria
[f] New Technologies-Research Center, University of West Bohemia, Univerzitni 8, 306 14 Pilson, Czech Republic
[g] Center of Excellence Geopolymer and Green Technology, School of Material Engineering, University Malaysia Perlis, 01007 Kangar, Perlis, Malaysia

ARTICLE INFO

Article history:
Received 12 February 2014
Accepted 27 February 2014
Available online 6 March 2014

Keywords:
Oxides
Ab initio calculations
Electronic properties
Optical spectra

ABSTRACT

We report ab initio density functional theory calculations of the structural, electronic and optical properties of the spinel oxides $SiMg_2O_4$, $SiZng_2O_4$, and $SiCd_2O_4$ using the full-potential linearized augmented plane-wave method. The structural parameters calculated using both the local density and generalized gradient approximations to the exchange-correlation potential are consistent with the literature data. To calculate the electronic properties, the exchange-correlation potential is treated with various functionals, and we find that the newly developed Tran–Blaha-modified Becke–Johnson functional significantly improves the band gap. We predict a direct band gap in all of the considered SiB_2O_4 compounds, and the band gaps continuously decrease as the atomic size of the B element increases. The decrease in the fundamental direct band gap (Γ–Γ) from $SiMg_2O_4$ to $SiZn_2O_4$ to $SiCd_2O_4$ can be attributed to p–d mixing in the upper valence bands of $SiZn_2O_4$ and $SiCd_2O_4$. The lowest conduction band is well dispersive, similar to that found for transparent conducting oxides such as ZnO. This band is mainly defined by the s and p electrons of the Si and B (B=Mg, Zn, Cd) atoms. The topmost valence band is considerably less dispersive and is defined by O-2p and B–d electrons. The charge-carrier effective masses are evaluated at the topmost valence band and at the bottommost conduction band that were calculated. The frequency-dependent complex dielectric function, absorption coefficient, refractive index, extinction coefficient, reflectivity and electron energy loss function were estimated. We find that the value of the zero-frequency limit of the dielectric function $\varepsilon(0)$ increases as the band gap decreases. The origins of the peaks and structures in the optical spectra are determined in terms of the calculated energy band structures.

1. Introduction

Spinel oxides are a family of ~120 compounds with the chemical formula AB_2O_4. In spinel oxides (AB_2O_4), there are two cations, A and B, in a 1:2 ratio, where A and B are either divalent and trivalent ($A^{II}B^{III}_2O_4$:A^{II}=Cd, Mg, Mn, Zn…, and B^{III}=Al, Ga, In…) or tetravalent and divalent cations ($A^{IV}B^{II}_2O_4$:A^{IV}=Si, Ge, Sn…, and B^{II}=Cd, Mg, Mn, Zn…). Cation A is surrounded by four oxygen ions, which forms an AO_4 tetrahedron, whereas cation B is surrounded by six oxygen ions, which forms an edge-sharing BO_6 octahedron (see Fig. 1). This structure has a cubic close packing (fcc) arrangement of oxide ions with a large unit cell that contains eight formula units ($A_8B_{16}O_{32}$) [1,2]. These spinel oxides possess many interesting electronic, mechanical, magnetic, and optical properties [3–36], which make them potential candidate materials for numerous technological applications. Consequently, these materials have been experimentally and theoretically investigated to better understand their fundamental properties. Among their interesting properties, the electronic and optical properties have attracted considerable attention, mainly because the knowledge of these properties is required to eventually apply these materials in optoelectronic devices.

* Corresponding author. Tel./fax: +213 36620136.
E-mail addresses: a_bouhemadou@yahoo.fr, abdelmadjidbouhemadou@gmail.com (A. Bouhemadou).

http://dx.doi.org/10.1016/j.physb.2014.02.053
0921-4526

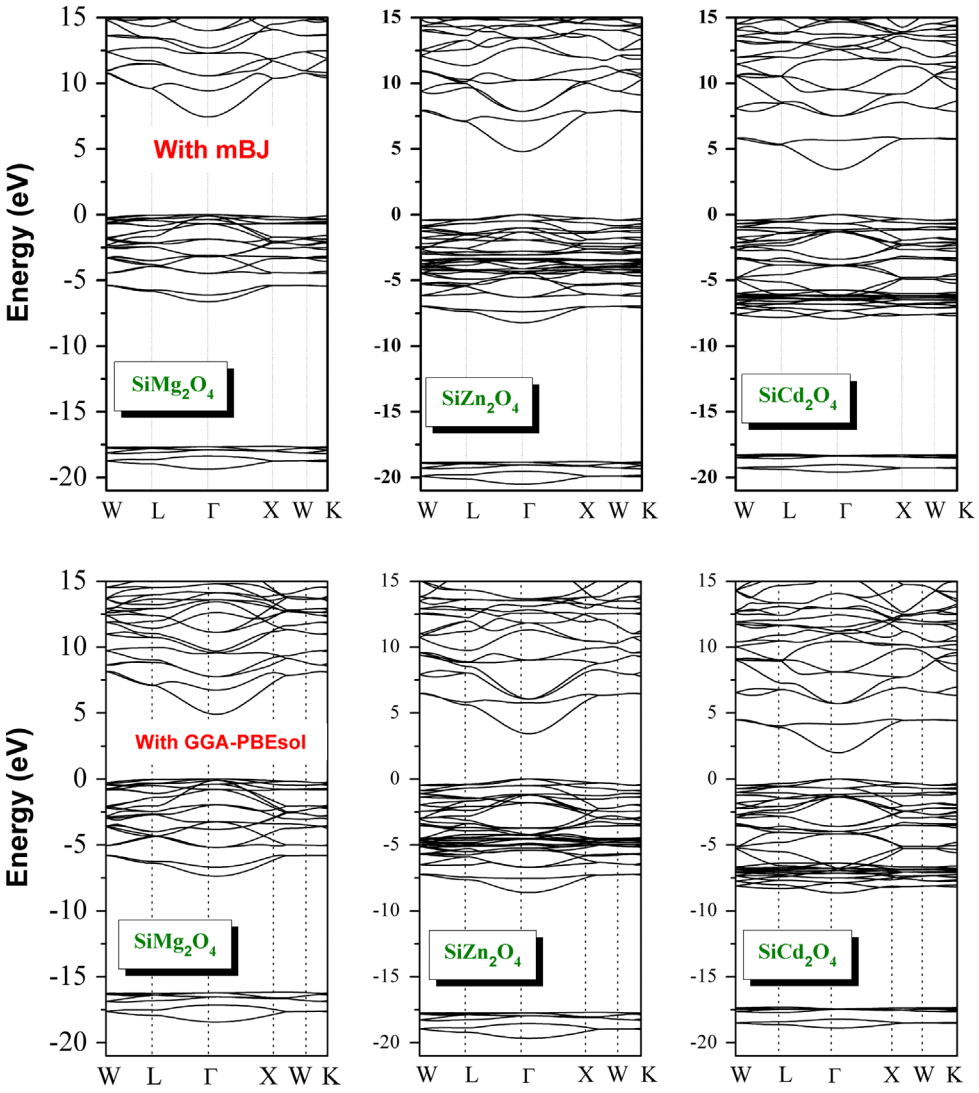

Fig. 1. Band structures of the spinel oxides $SiMg_2O_4$, $SiZn_2O_4$ and $SiCd_2O_4$ along the high-symmetry directions calculated using the GGA-PBEsol and TB-mBJ functionals. The Fermi level is shifted to zero.

The recent growing demand for high-performance, low-cost transparent conducting oxides (TCOs) in optoelectronic devices, such as flat-panel displays, windshield defrosters and solar cells [3,4], has led to an extensive search for new TCO materials with higher transparency and conductivity [5]. There has been considerable work involving both experimental and theoretical methods on the $A^{II}B_2^{V}O_4$ spinel oxides, such as $MgAl_2O_4$, $ZnAl_2O_4$, and $ZnGa_2O_4$ [5–36], but there are very few reports on the $A^{IV}B_2^{II}O_4$ spinel oxides, such as $SiMg_2O_4$, $SiZn_2O_4$, and $SiCd_2O_4$. In particular, the only known properties of the $SiMg_2O_4$, $SiZn_2O_4$, and $SiCd_2O_4$ materials are their structural properties [6,37], elastic constants [37], lattice dynamics (only for $SiMg_2O_4$) [38], and electronic structure properties [37]. We are unaware of any studies of the optical properties of the spinels considered herein. Previous theoretical studies [6,37,38] were performed within the density functional theory (DFT) framework [39,40] with the standard local density approximation (LDA) and the generalized gradient approximation (GGA), which are known to severely underestimate the band gaps of semiconductor and insulator materials [41]. Indeed, DFT with the common LDA and GGA yields satisfactory structural parameters that are fairly consistent with the experimental values, but it provides unsatisfactory electronic properties (such as the band gap and effective masses). The band gaps calculated using DFT with the common LDA and GGA are likely to be approximately 30–50% smaller than the experimental values [42].

Currently, some approximations beyond the LDA and GGA, such as GW, hybrid functionals (B3LYP, HSE…), LDA+U, LDA+DMFT, etc., have been developed to accurately describe the electronic structures of semiconductors and insulators. However, some of these methods are computationally expensive or not satisfactory in all cases [43]; for example, the LDA+U method can only be applied to correlated and localized electrons. Fortunately, a very elegant approach to solve this dilemma has recently been suggested by Tran and Blaha [44–46]; the so-called Tran–Blaha-modified Becke–Johnson (TB-mBJ) potential approximation is implemented in the new version of the WIEN2K code [47]. The TB-mBJ is an alternative method to have a band gap close to the experimental value, and it is computationally cheaper than the other mentioned methods. For spinel oxides, the TB-mBJ method has been demonstrated to obtain band gaps that are consistent with the more accurate results obtained using the GW method [36,48]. Tran and Blaha [43] demonstrated that the TB-mBJ potential yields band gaps that are consistent with the experimental values, which leads to typical errors of less than 10% for some semiconductors and insulators. The drawback of the TB-mBJ potential is that it cannot be obtained as the derivative of an exchange-correlation function [43]. Therefore, this potential cannot be used to calculate properties that depend on energy, such as the structural properties.

In this work, we aim to calculate the electronic properties of the $SiMg_2O_4$, $SiZn_2O_4$ and $SiCd_2O_4$ materials using the LDA [49], GGA-PBEsol [50] and Engel–Vosko scheme of the GGA (GGA-EV) [51] functionals. In addition, we aim to compare these properties to the results obtained using the TB-mBJ functional [44–46] to demonstrate the advantage of the TB-mBJ method for describing the electronic structure of the considered materials. Another objective of the present work is to explore in detail the optical properties of the spinel oxides $SiMg_2O_4$, $SiZn_2O_4$, and $SiCd_2O_4$ for this first time. This paper is organized as follows: in Section 2, the calculation method is briefly outlined. The obtained results and some discussions are presented in Section 3. Finally, some concluding remarks are provided in Section 4.

2. Methodology

All of the electronic total energy calculations in this work were performed in the framework of density functional theory (DFT) and with an all-electron method with the linearized/augmented plane wave+local orbitals (L/APW+lo) basis set as implemented in the WIEN2k code [47]. In this method, the wave functions are expanded in a linear combination of radial functions time spherical harmonics inside the non-overlapping muffin-tin spheres of radius R_{MT} surrounding each atom and in plane waves in the interstitial region between the spheres. The radii of the muffin-tin spheres were taken as large as possible without overlapping the spheres. The maximum l of the expansion of the wave function in spherical harmonics inside the muffin-tin spheres was $l_{max}=10$. A plane-wave cut-off of $K_{max}=4.0$ a.u.$^{-1}$ is chosen for the expansion of the wave functions in the interstitial region. The k integrations over the Brillouin zone (BZ) are performed up to $10\times10\times10$ Monkorst–Pack mesh (MP) [52] (47 k-points in the irreducible Brillouin zone (IBZ)). The self-consistent calculations are considered converged when the total energy of the system is stable within 10^{-5} Ry. The atomic positions were relaxed until the forces were below 0.5 mRy a.u.$^{-1}$. The exchange-correlation potential for the structural properties was calculated using the LDA [49] and the GGA based on Perdew et al. (GGA-PBEsol) [50]. For the electronic properties, in addition to the LDA and the GGA, the GGA-EV [51] and the TB-mBJ [44–46], which better describe many semiconductors and insulators, were applied.

3. Results and discussion

3.1. Structural properties

SiB_2O_4 (B=Mg, Zn, and Cd) spinel oxides crystallize in the cubic spinel structure with the space group $Fd\bar{3}m$ (No. 227). The unit cell contains 56 atoms: 8 silicon atoms, which occupy the tetrahedral sites of Wyckoff position 8a (0.125, 0.125, 0.125); 16 B atoms at the octahedral sites of position 16d (0.5, 0.5, 0.5); and 32 oxygen atoms at position 32e (u, u, u). Therefore, the cubic spinel structure is characterized by two free structural parameters that are not fixed by symmetry: the lattice constant (a) and the coordinate of the oxygen atom (u). The optimized lattice constant and the oxygen positional parameter were determined variationally using the previously given calculation settings (Section 2).

In Table 1, we show the obtained results for the lattice constant a, the internal coordinate u, the bulk modulus B and the pressure derivative of the bulk modulus B' using both the local density [49] (LDA) and the generalized gradient [50] (GGA) approximations to the exchange-correlation potential and compare these values with the available experimental and theoretical data. As shown in Table 1, our calculated lattice constant of $SiMg_2O_4$ (the only compound for which experimental data are available in the literature) is consistent with the reported measured one. The LDA yields a lattice constant value that is slightly below (−0.8%) the experimental value, whereas the GGA gives a value that is slightly above (+0.2%). In addition, the theoretical results reported by other researchers [6,36,37] are also consistent with one another. This consistency proves the reliability and the accuracy of these present ab initio calculation findings and gives confidence in the results of the following calculations of the electronic and optical properties for the considered materials. We did not find any experimental results for B and B' in the literature to support these theoretical results. Our B and B' values obtained using the FP-L/APW+lo method are reasonably consistent with those obtained using the pseudopotential plane-wave (PP-PW) method [36].

Table 1
Calculated lattice constant a_0 (in), internal coordinate of the oxygen atom u, bulk modulus B (in GPa), and the pressure derivative of the bulk modulus B' for the $SiMg_2O_4$, $SiZn_2O_4$ and $SiCd_2O_4$ compounds in comparison with the available experimental and theoretical results in the literature [6,36,37].

	$SiMg_2O_4$			$SiZn_2O_4$		$SiCd_2O_4$	
	Present	Expt.	Others	Present	others	Present	Others
a_0	8.0877[a] 8.0006[d]	8.0709[b]	8.1318[c] 8.0351[c] 8.039[e] 8.1385[b]	8.1526[a] 8.0644[d]	8.1718[c] 8.0499[c] 8.0830[e]	8.7048[a] 8.6132[d]	8.7504[c] 8.6164[c] 8.6170[e]
u	0.2442[a] 0.2446[d]		0.2419[c] 0.24315[c] 0.2442[e]	0.2430[a] 0.2435[d]	0.2409[c] 0.2427[c] 0.2432[e]	0.2357[a] 0.2359[d]	0.2333[c] 0.2349[c] 0.2362[e]
B_0	183.68[a] 197.73[d]		169[c] 193[c]	204.58[a] 221.61[d]	186[c] 206[d]	169.39[a] 190.24[d]	155[c] 191[c]
B'	3.95[a] 4.05[d]		4.32[c] 3.80[c]	4.21[a] 4.47[d]		4.72[a] 4.62[d]	5.0[c] 4.35[c]

[a] Present work using the GGA-PBEsol.
[b] Ref. [37].
[c] Ref. [36].
[d] Present work using the LDA.
[e] Ref. [6].

3.2. Electronic properties

Now, we discuss our results of the electronic properties of $SiMg_2O_4$, $SiZn_2O_4$ and $SiCd_2O_4$ via the energy bands, density of states and charge-carrier effective masses. The electronic band structures are calculated with the optimized crystal structure parameters for all three considered materials using four different functionals: the LDA, the GGA-PBEsol, the GGA-EV and the TB-mBJ. It is well known that the common LDA and GGA usually severely underestimate the energy band gap [54]. Engel and Vosko [51] considered this shortcoming and constructed a new functional form of the GGA (denoted here as EV-GGA), which was designed to provide a better exchange-correlation potential. This approach (EV-GGA) yields better band splitting and some other properties that mainly depend on the accuracy of the exchange-correlation potential. The recently proposed Tran–Blaha-modified Becke–Johnson (TB-mBJ) potential approximation [44–46] as implemented in Wien2K [47] yields band gaps consistent with the experiment, which leads to typical errors of less than 10% for some semiconductors and insulators [43]. Note that because there is no exchange and correlation energy term from which the mBJ potential can be deduced, a direct optimization procedure is not possible as in the usual theory [53]. The GGA-EV functional is obtained by optimizing the exchange-correlation potential V_{ex} rather than the energy V_{ex}, and it is designed to improve the band

Table 2
Calculated fundamental band gap energy E_g (in eV) using four different approaches for the exchange-correlation potential: LDA, GGA-PBEsol, GGA-EV and TB-mBJ in comparison with the available theoretical results.

System	Present work				Other [36]	
	LDA	GGA-PBEsol	GGA-EV	TB-mBJ	LDA	GGA
$SiMg_2O_4$	5.26	4.90	5.92	7.43	5.01	5.19
$SiZn_2O_4$	2.84	2.56	3.43	4.70	2.77	2.90
$SiCd_2O_4$	1.36	1.18	1.98	3.43	1.17	1.34

gaps rather than the local energy. Consequently, the equilibrium lattice constant calculated using this functional is considerably larger than the experimental value [54]. Therefore, the band structures using the TB-mBJ and GGA-EV functionals were calculated with the lattice parameter values that were obtained using the GGA-PBEsol functional.

In Fig. 1, we compare the band structures calculated using the GGA-PBEsol and TB-mBJ functionals for the $SiMg_2O_4$, $SiZn_2O_4$ and $SiCd_2O_4$ compounds along the high symmetry lines in the corresponding Brillouin zone. In general, the TB-mBJ potential causes a rigid displacement of the conduction bands toward higher energy with small differences in the dispersion at some regions of the Brillouin zone. Both the maximum of the valence band (VBMa) and the minimum of the conduction band (CBMi) are located at the Γ point (the Brillouin zone center) for the three studied compounds, which allows us to classify these spinel oxides as direct band gap materials. The calculated fundamental band gaps of the three considered materials using four different functionals (LDA, GGA-PBEsol, GGA-EV and TB-mBJ) are listed in Table 2 along with a comparison with previous theoretical results. Our direct energy band gap (Γ–Γ) calculated using the LDA and the GGA-PBEsol methods compares favorably with that obtained using the same functional [36]. The experimental band gap values for these oxides are not yet available for comparison with our predicted values. However, we can assess the obtained results using the published material regarding the accuracy of each different functional. Because the band gaps that were calculated using the DFT with the common LDA and GGA are likely approximately 30–50% smaller than the experimental values [55], it is clear from Table 2 that our band gaps calculated using the TB-mBJ potential are significantly improved compared to the other exchange-correlation functionals. The fundamental band gaps for the considered oxides calculated using the TB-mBJ approach are in the range of 3.43–7.73 eV. Hence, these materials are classified as wide-band-gap solids and are consequently transparent in the visible spectra. From the band structures, one can observe that the maxima of the valence bands are flat, which indicates that they have large hole effective masses. Thus, the p-type materials should have some unusual transport properties.

To study the nature of the energy band structures of the $SiMg_2O_4$, $SiZn_2O_4$ and $SiCd_2O_4$ compounds in the TB-mBJ functional, the total density and the atomic site projected density of states (TDOS and PDOS) of these compounds are explored. The TDOS and PDOS diagrams of $SiMg_2O_4$, $SiZn_2O_4$ and $SiCd_2O_4$ are depicted in Fig. 2. Because the DOS diagrams of the three considered compounds are similar, we detailed only the density of electronic states of $SiMg_2O_4$ as an example. The lower group of valence bands, which are not shown here for clarity, extending around −39.0 to −38.53 eV, is due to the Mg-2p states. The structure localized between −18.49 and −16.12 eV below the Fermi level mainly consists of the O-2s states with contributions from the Mg-3s and Si-3s3p states. The region near the Fermi level, i.e., the top of the valence band, extends to approximately −7.45 to 0 eV and has predominantly O-2p-like character. The substitution of Mg by Zn (Cd) in the $SiZn_2O_4$ ($SiCd_2O_4$) compound introduces a contribution from the Zn-3d (Cd-4d) states to the upper valence band. Rather than the O-2p-dominated states in $SiMg_2O_4$, the zinc 3d states (cadmium 4d states) appear in the upper valence band of $SiZn_2O_4$ ($SiCd_2O_4$); consequently, its width broadens to 8.53 eV. Therefore, changes in the electronic properties of $SiZn_2O_4$ ($SiCd_2O_4$) compared with those of $SiMg_2O_4$ would be solely because of the mixing of the Zn-3d (Cd-4d) and O-2p orbitals. In the three compounds, the bottom of the conduction band is composed of the s and p states of Si and B (B=Mg, Zn, and Cd) atoms.

Generally, a decrease in the band gap is expected with the substitution of cations by heavier cations (e.g., Zn for Mg and Cd for Zn) in a series of structurally isomorphous compounds [15]. The calculated results show a decrease in the gap in the following sequence: $Eg(SiMg_2O_4) > Eg(SiZn_2O_4) > Eg(SiCd_2O_4)$ (see Table 2). The role of the d states in defining the electronic properties of the II–VI semiconductors [56], zinc aluminates [6], zinc aluminates, zinc gallate [15] and cubic spinels AB_2O_4, where A=Si and Ge, and B=Mg, Zn and Cd [37,57], has been discussed. It has been reported that the p–d hybridization at Γ repels the valence band maximum upwards without affecting the conduction band minimum. Hence, the decrease of the calculated direct gap Γ–Γ from 7.43 eV in $SiMg_2O_4$ to 4.70 eV in $SiZn_2O_4$ and to 3.43 eV in $SiCd_2O_4$ (using TB-mBJ) can be attributed to the presence of the 3d and 4d states in $SiZn_2O_4$ and $SiCd_2O_4$, respectively.

The pressure dependence of the size of the fundamental energy band gaps of $SiMg_2O_4$, $SiZn_2O_4$ and $SiCd_2O_4$ was investigated. The calculated band gaps for the three considered materials are well fitted to a quadratic polynomial: $E_g(P) = E_g(0) + \alpha P + \beta P^2$, where $E_g(0)$ is the band gap at zero pressure, P is the pressure, and α and β are the linear and the quadratic pressure coefficients, respectively. The obtained coefficients are as follows:

$$\alpha(SiMg_2O_4) = 5.36 \times 10^{-2}\ \text{eV/GPa},$$
$$\beta(SiMg_2O_4) = -1.535 \times 10^{-4}\ \text{eV/GPa}^2,$$
$$\alpha(SiZng_2O_4) = 3.04 \times 10^{-2}\ \text{eV/GPa},$$
$$\beta(SiZng_2O_4) = -0.885 \times 10^{-4}\ \text{eV/GPa}^2,$$
$$\alpha(SiCd_2O_4) = 3.64 \times 10^{-2}\ \text{eV/GPa} \quad \text{and}$$
$$\beta(SiCd_2O_4) = -1.445 \times 10^{-4}\ \text{eV/GPa}^2.$$

The energy band gaps of the studied compounds increase as the pressure is increased.

The effective charge-carrier mass is one of the main factors that determine the transport properties and electrical conductivity of a material. In general, smaller effective masses of the carriers correspond to the faster photogenerated carriers. Consequently, a low effective mass can promote carrier migration and suppress carrier recombination. Here, the effective charge-carrier mass m^* was evaluated by fitting the E–k diagram near the valence-band maximum (VBMa) and the conduction-band minimum (CBMi) with a paraboloid. The effective mass m^* (in unit of m_0, where m_0 denotes the electron rest mass) at a given point along the direction given by $\vec{k}$ is

$$\frac{1}{m^*} = \frac{m_0}{h^2}\frac{\partial^2 E(k)}{\partial^2 k}$$

The evaluated effective charge-carrier masses at the Γ point from the band dispersions of the VBMa and CBMi towards the X and L directions in the Brillouin zone are summarized in Table 3 for the three considered materials. The effective electron mass, the heavy-hole mass and the light-hole mass are indicated by the subscripts "e" (m_e^*),"hh" (m_{hh}^*), and "hl" (m_{hl}^*), respectively. The calculated CB electron effective masses of the considered oxides are slightly higher than those of some known transparent conducting oxides (TCOs). For example, the CB electron effective mass is 0.23 [58] and

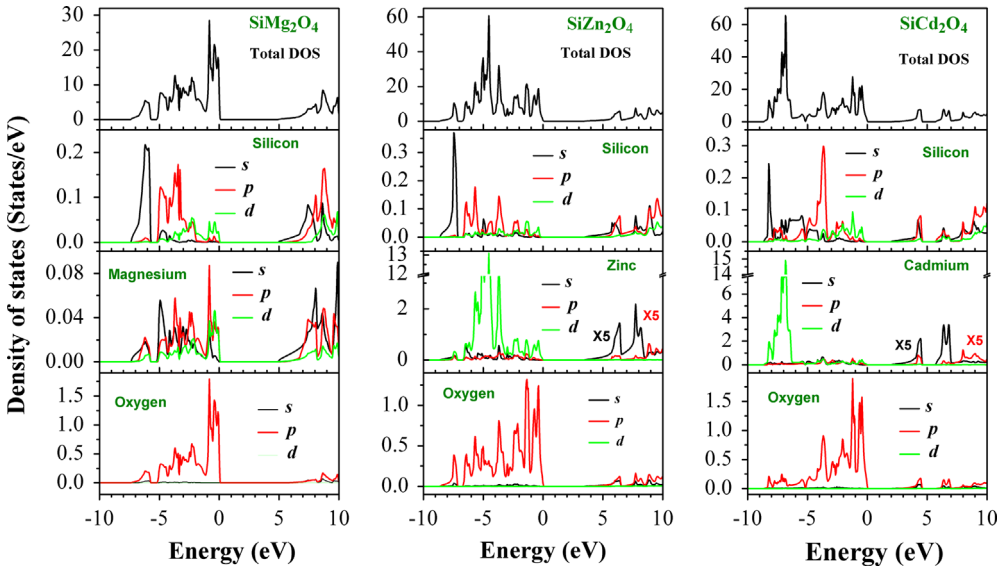

Fig. 2. Diagrams of the total and the site-projected density of state for the spinel oxides $SiMg_2O_4$, $SiZn_2O_4$ and $SiCd_2O_4$ as calculated using the TB-mBJ functional. The Fermi level is shifted to zero.

Table 3
Calculated effective masses of the electron m_e^*, the heavy hole m_{hh}^*, and the light hole m_{lh}^* (in units of the free electron mass m_0) for the $SiMg_2O_4$, $SiZn_2O_4$ and $SiCd_2O_4$ compounds using the TB-mBJ functional.

Direction	$SiMg_2O_4$	$SiZn_2O_4$	$SiCd_2O_4$
m_e^*/m_0 (Γ–X)	0.46	0.45	0.40
m_e^*/m_0 (Γ–L)	0.47	0.41	0.40
m_{lh}^*/m_0 (Γ–X)	1.23	1.04	1.09
m_{lh}^*/m_0 (Γ–L)	3.96	1.21	1.19
m_{hh}^*/m_0 (Γ–X)	8.36	4.80	4.01
m_{hh}^*/m_0 (Γ–L)	4.09	2.40	2.49

0.24 [59] for ZnO, 0.35 for $SnMg_2O_4$, 0.23 for $SnZn_2O_4$ and 0.20 for $SnCd_2O_4$ [60]. Consequently, the mobility of the CB electrons and the electrical conductivity in the considered materials should be slightly small. From Table 3, we note that (i) the electronic states at the conduction-band minimum are much more dispersive than the topmost valence-band states; consequently, the conduction-band electrons have lower effective masses than the valence-band holes, and the influence of the latter on the electrical conductivity is minimal; (ii) the effective masses of electrons in the considered materials for the $\Gamma \rightarrow X$ and $\Gamma \rightarrow L$ directions in the BZ are practically equal; hence, the conduction-band electron mobility and the electrical conductivity of the studied materials should be isotropic; (iii) the heavy holes have higher effective masses than the light holes, which indicates the anisotropy between heavy- and light-hole masses; (iv) the valence-band maximum is flat, which represents the rather large effective masses of the heavy holes; and (iiv) the dependence of the effective masses of the holes on the crystallographic direction demonstrates the anisotropy of this property; hence, the valence-band hole conductivity should also be anisotropic.

3.3. Optical properties

The optical properties of a material are usually described by the complex dielectric function $\varepsilon(\omega) = \varepsilon_1(\omega) + i\varepsilon_2(\omega)$, which characterizes the linear response of a material to electromagnetic radiation and governs the propagation behavior of radiation in a medium. The imaginary part of the dielectric function $\varepsilon_2(\omega)$ represents the absorption in the crystal, which can be calculated from the momentum matrix elements between the occupied and the unoccupied wave functions [61]. Then, the real part of the dielectric function $\varepsilon_1(\omega)$, which determines how the electromagnetic energy is dispersed when it penetrates a medium, is evaluated from the imaginary part $\varepsilon_2(\omega)$ using the Kramers–Kronig transformation. Using both the real part and the imaginary part of the dielectric function, one can calculate the other important linear optical properties, such as the refractive index $n(\omega)$, the extinction coefficient $k(\omega)$, the optical reflectivity $R(\omega)$, the absorption coefficient $\alpha(\omega)$ and the electron energy-loss spectrum $L(\omega)$. The optical property calculation requires a dense mesh of energy eigenvalues and the corresponding eigenvectors; therefore, a dense mesh of uniformly distributed k-points must be used to calculate the optical constants. Because $\varepsilon_2(\omega)$ is usually calculated first, we chose it to be a reference to assess the convergence. The calculation converges for a $30 \times 30 \times 30$ Monkhorst–Pack k-point sampling procedure [52]; therefore, a $30 \times 30 \times 30$ k-mesh was used to calculate the optical properties. We used the Tran–Blaha-modified Becke–Johnson functional alone to calculate the optical properties because of the improved band gap.

The calculated imaginary part $\varepsilon_2(\omega)$ of the frequency-dependent dielectric function for the studied compounds using the TB-mBJ functional in the energy range of 0–30 eV is presented in Fig. 3. It would be useful to attempt to identify the electronic transitions that are responsible for the spectral structures in the optical spectra. The imaginary part of the dielectric function is determined by the allowed electronic transitions between each pair of occupied and unoccupied bands. Therefore, the origins of different peaks and features of the optical spectra are determined by decomposing each spectrum to its individual pair contribution, i.e., the contribution from each electronic transition from the occupied valence state V_i to the empty conduction state C_j ($V_i \rightarrow C_j$) and plotting the electronic transition energy $E_{ij}(k) = E_{C_j}(k) - E_{V_i}(k)$ band structures along the high-symmetry directions in the Brillouin zone. These techniques inform us about the bands that contribute more to the peaks of the $\varepsilon_2(\omega)$ spectrum and their locations in the Brillouin zone. The main contributions to the optical spectra originate from the top valence bands to the lower conduction bands. In Fig. 4, the top panel shows the dominant contributions to $\varepsilon_2(\omega)$ from the interband transitions, and the bottom panel shows the locations of these transitions in the Brillouin zone for $SiMg_2O_4$. The first critical point E_0 of $\varepsilon_2(\omega)$ is the edge of the optical absorption. This point is the $\Gamma_V - \Gamma_C$ splitting,

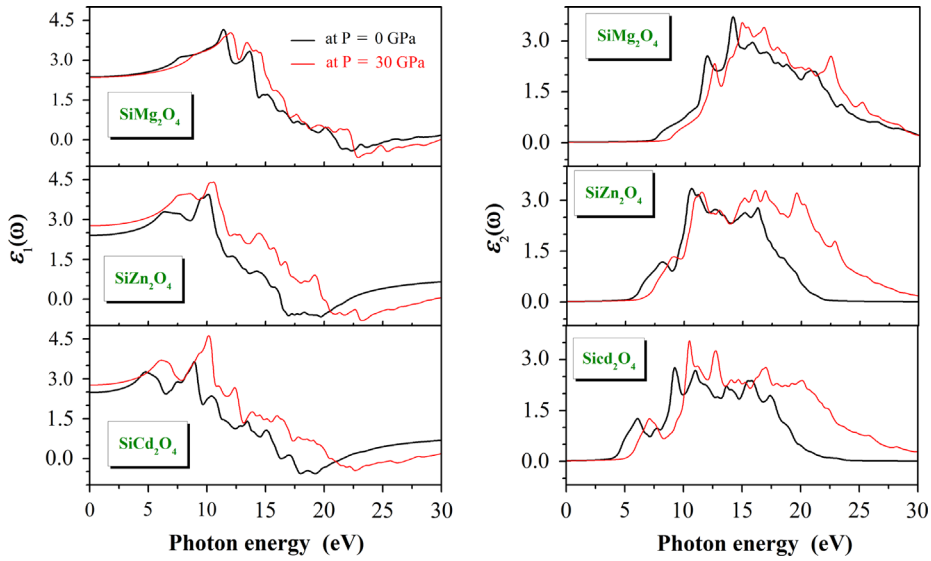

Fig. 3. Real (left panel; $\varepsilon_1(\omega)$) and imaginary (right panel; $\varepsilon_2(\omega)$) parts of the dielectric function of the spinel oxides $SiMg_2O_4$, $SiZn_2O_4$ and $SiCd_2O_4$ as calculated using the TB-mBJ functional.

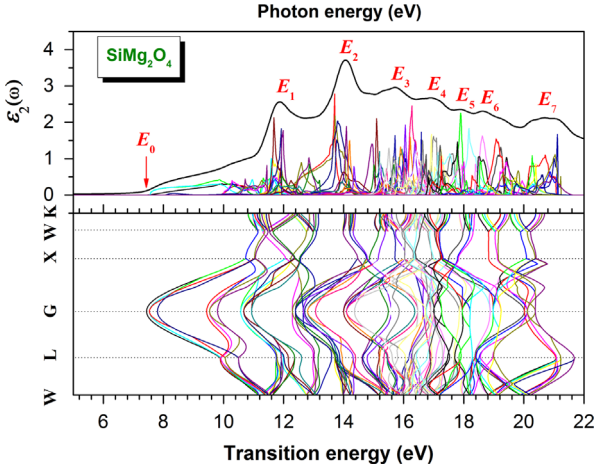

Fig. 4. Decomposition of the imaginary part $\varepsilon_2(\omega)$ of the dielectric function into the band-to-band contributions (upper panel) and the transition energy band structure (lower panel) for $SiMg_2O_4$.

which gives the threshold of the direct optical transition between the topmost valence band V_1 and the bottommost conduction band C_1 ($V_1 \rightarrow C_1$ transition); the counting of the bands is down (up) from the top (bottom) of the valence (conduction) band. This edge is known as the fundamental absorption edge. This first critical point is followed by a broad shoulder at approximately 7.5–11 eV because of the $V_3 \rightarrow C_1$, $V_1 \rightarrow C_1$, $V_4 \rightarrow C_1$ and $V_2 \rightarrow C_1$ transitions and some structures centered at the E_i points. The previously described techniques were applied for the $\varepsilon_2(\omega)$ spectra of all three investigated compounds. Because the results are notably similar, we show only the decomposition of the $\varepsilon_2(\omega)$ spectrum of $SiMg_2O_4$ in Fig. 4. The locations of the major peaks E_i with the dominant contributions from the interband transitions to each peak and their locations in the Brillouin zone for all three compounds are reported in Tables 5–7. We note that all structures in the $\varepsilon_2(\omega)$ spectrum are shifted toward lower energy as we observe from $SiMg_2O_4$ to $SiZn_2O_4$ to $SiCd_2O_4$. This trend may be directly inferred from the band structure results because the band gap energy decreases from $SiMg_2O_4$ to $SiZn_2O_4$ to $SiCd_2O_4$.

The dispersive part $\varepsilon_1(\omega)$ of the dielectric function for $SiMg_2O_4$, $SiZn_2O_4$ and $SiCd_2O_4$ is calculated from the imaginary part $\varepsilon_2(\omega)$ of the frequency-dependent dielectric function according to the

Table 4
Calculated static dielectric constant $\varepsilon_1(0)$, static refractive index $n(0)$, and pressure coefficients of the refractive index $n(0)$ for the $SiMg_2O_4$, $SiZn_2O_4$ and $SiCd_2O_4$ compounds.

System	$\varepsilon_1(0)$	$n(0)$	E($n=1$)	$\frac{1}{n_0}\frac{dn}{dp}(10^{-5}\ GPa^{-1})$
$SiMg_2O_4$	2.195	1.479	18.88	−2.43
$SiZn_2O_4$	2.396	1.548	16.62	−2.56
$SiCd_2O_4$	2.483	1.682	19.82	−2.68

Kramers–Kronig dispersion relation and is also shown in Fig. 3. The intensity of the highest peak in the $\varepsilon_1(\omega)$ spectrum decreases from $SiMg_2O_4$ to SiZ_2O_4 to $SiCd_2O_4$. The static dielectric constant $\varepsilon_1(0)$ is given by the low energy limit of $\varepsilon_1(\omega)$. The calculated static dielectric constants $\varepsilon_1(0)$ of the considered materials are listed in Table 4. We find that the values of $\varepsilon_1(0)$ increases as the energy gap E_g decreases. This result can be explained based on the Penn model [62,63]. The Penn model is based on the expression $\varepsilon_1(0) \approx 1 + (\hbar\omega_p/E_g)^2$, where $\hbar\omega_p$ is the plasma energy. It is clear that $\varepsilon_1(0)$ is inversely proportional to E_g. Hence, a smaller E_g yields a larger $\varepsilon_1(0)$.

When these materials are compressed, the positions of all previously mentioned critical points are shifted with an enhanced energy comparable to that at zero pressure. The reason for this behavior is the enhancement of the direct band gaps under pressure. Although their positions are shifted under pressure, these points still have the same type as that at zero pressure. Fig. 5 shows the pressure dependence of the static dielectric constant $\varepsilon_1(0)$ for the $SiMg_2O_4$, $SiZn_2O_4$ and $SiCd_2O_4$ materials. The symbols show the ab initio results for the given pressures. The lines are the second-order polynomial fit to the results. The fitting results (quadratic equations) for the static dielectric constant $\varepsilon_1(0)$ are given by the following expressions:

$$SiMg_2O_4 : \varepsilon_1(0) = 2.1951 - 0.00789P + 4.57143 \times 10^{-5}P^2$$

$$SiZn_2O_4 : \varepsilon_1(0) = 2.3956 - 0.01089P + 3.2857 \times 10^{-5}P^2$$

$$SiCd_2O_4 : \varepsilon_1(0) = 2.4825 - 0.01055P + 2.57143 \times 10^{-5}P^2$$

The calculated refractive index $n(\omega)$ and the extinction coefficient $k(\omega)$ as functions of the photon energy are displayed in Fig. 6. For lower energies, the refractive index values are almost constant and begin to increase at energies near the absorption edge to

Table 5
Peak positions of the imaginary part of the dielectric function $\varepsilon_2(\omega)$ with the dominant interband transition contributions to every peak and their locations in the Brillouin zone for $SiMg_2O_4$.

Optical structures		Dominant interband transition contributions		
Structure	Peak position	Transition	Region	Energy (eV)
E_0	7.43	(V_1–C_1)	Γ–Γ	
E_1	11.88	(V_1–C_1)	W–L, Γ–X	9.96, 10.21
		(V_1–C_2)	W–L, Γ–X–W–K	10.50, 10.98
		(V_1–C_3)	W–L–Γ–X–W	11.36
		(V_1–C_4)	W–L–Γ–X–W–K	11.71
		(V_1–C_5)	L–Γ–X	11.94
		(V_1–C_6)	Γ–X–W	12.27
		(V_2–C_2)	W–L, Γ–X–W	10.31, 10.92
		(V_2–C_3)	W–L–Γ–X–W	11.59
		(V_2–C_4)	W–L–Γ–X–W–K	11.71
		(V_2–C_5)	W–L, Γ–X	12.04
		(V_2–C_6)	L–Γ, X–W	12.63
		(V_3–C_1)	W–L, Γ–X, W–K	11.00
		(V_3–C_2)	W–L, Γ–X–W	10.36, 11.36
		(V_3–C_3)	W–L–Γ–X–W	11.59
		(V_3–C_4)	W–L, Γ–X –W–K	11.93
		(V_3–C_5)	W–L, Γ–X	12.04
		(V_4–C_2)	W–L, Γ–X–W–K	11.23
		(V_4–C_3)	Γ–X–W	11.94
		(V_5–C_2)	W–L–Γ–X–W	10.67,11,46
		(V_5–C_3)	W–L–Γ–X –W	11.71
E_2	14.04	(V_1–C_7)	L–Γ–X	13.67
		(V_1–C_8)	L–Γ–X	13.67
		(V_1–C_9)	L–Γ–X	13.78
		(V_1–C_{10})	W–L, Γ–X–W	14.93
		(V_2–C_7)	W–L, Γ–X	13.78
		(V_2–C_8)	Γ–X–W	14.14
		(V_2–C_9)	W–L, Γ–X	14.01
		(V_2–C_{10})	W–L, Γ–X–W	15.05
		(V_3–C_7)	W–L, Γ–X	14.01
		(V_3–C_8)	W–L, Γ–X	14.13
		(V_3–C_9)	W–L, Γ–X	14.36
		(V_4–C_7)	W–L, Γ–X	13.90
		(V_4–C_8)	W–L, Γ–X–W–K	14.24
		(V_4–C_9)	W–L, Γ–X	14.24
		(V_5–C_7)	L–Γ–X	14.14
		(V_5–C_8)	Γ–X–W–K	14.36
		(V_5–C_9)	L–Γ–X	14.16
E_3	15.71	(V_1–C_{11})	L–Γ–X	15.05
		(V_1–C_{12})	W–L, Γ–X–W	15.64
		(V_1–C_{13})	W–L–Γ–X–W–K	15.97
		(V_1–C_{14})	W–L, Γ–X–W–K	13.78
		(V_1–C_{15})	W–L, Γ–X–W–K	16.20
		(V_2–C_{11})	L–Γ–X	15.18
		(V_2–C_{12})	W–L, Γ–X	15.74
		(V_2–C_{13})	W–L–Γ–X–W–K	15.87
		(V_3–C_{11})	W–L, Γ–X	15.28
		(V_3–C_{12})	W–L, Γ–X, W–K	15.74
		(V_3–C_{13})	W–L–Γ–X–W–K	15.98
		(V_4–C_{12})	W–L, Γ–X, W–K	15.74
		(V_4–C_{13})	W–L–Γ–X	15.64
		(V_5–C_9)	W–L, X–W	15.30
		(V_5–C_{10})	W–L–Γ–X–W	15.28
E_4	16.95	(V_1–C_{16})	W–L–Γ–X, W–K	16.33
		(V_1–C_{17})	W–L, Γ–X, W–K	16.66
		(V_1–C_{18})	W–L	16.56
		(V_2–C_{14})	W–L, Γ–X, W–K	16.10
		(V_2–C_{15})	W–L, Γ–X, W–K	16.20
		(V_2–C_{16})	W–L–Γ–X	16.43
		(V_2–C_{17})	Γ–X, W–K	16.56
		(V_2–C_{18})	W–L–Γ–X	17.02
		(V_2–C_{19})	W–L–Γ–X	17.25
		(V_3–C_{17})	W–L–Γ–X, W–K	16.91
		(V_3–C_{18})	W–L–Γ–X–W	17.14
		(V_3–C_{19})	W–L–Γ–X–W–K	17.25
		(V_4–C_{14})	W–L, Γ–X, W–K	16.33
		(V_4–C_{15})	W–L, Γ–X, W–K	16.43
		(V_4–C_{16})	L–Γ–X	16.91
		(V_5–C_{14})	W–L–Γ–X–W–K	16.33, 16.87
		(V_5–C_{15})	W–L–Γ–X–W–K	16.52, 17.00
		(V_5–C_{16})	W–L, Γ–X	16.79
		(V_5–C_{17})	W–K	16.79
E_5	17.89	(V_1–C_{19})	W–L–Γ–X, W–K	17.14
		(V_1–C_{20})	W–L, Γ–X	17.60
		(V_1–C_{21})	W–L, Γ–X–W–K	17.94
		(V_2–C_{20})	W–L, Γ–X	17.52
		(V_2–C_{21})	W–L–Γ–X–W–K	17.94
		(V_3–C_{20})	L–Γ–X	17.83
		(V_3–C_{21})	W–L–Γ–X–W	17.94
		(V_3–C_{22})	Γ–X–W	18.17
		(V_3–C_{23})	W–L–Γ	18.52
		(V_4–C_{18})	W–L–Γ–X	17.25
		(V_4–C_{19})	L–Γ–X	17.48
		(V_4–C_{20})	W–L, Γ–X	17.77
		(V_4–C_{21})	W–L–Γ–X–W	18.06
		(V_5–C_{18})	W–L, Γ–X–W	17.25
		(V_5–C_{19})	W–L–Γ–X–W–K	17.29, 17.64
		(V_5–C_{20})	W–L, Γ–X, W–K	17.48, 17.96
E_6	18.63	(V_1–C_{22})	W–L, Γ–X	18.17
		(V_1–C_{23})	W–L–Γ, W–K	18.65
		(V_1–C_{24})	W–L–Γ–X, W–K	19.21
		(V_2–C_{22})	W–L, Γ–X	18.17
		(V_2–C_{23})	W–L–Γ, W–K	18.52
		(V_2–C_{24})	W–L–Γ–X, W–K	19.11
		(V_2–C_{25})	W–L, Γ–X	19.44
		(V_4–C_{22})	W–L, Γ–X	18.29
		(V_4–C_{24})	W–L–Γ–X	19.44
		(V_5–C_{21})	W–L, Γ–X–W	18.29
		(V_5–C_{22})	W–L–Γ–X–W–K	18.52
		(V_5–C_{23})	W–L, Γ–X, W–K	18.88
		(V_5–C_{24})	W–L–Γ–X, W–K	19.27
E_7	20.70	(V_1–C_{25})	W–L, Γ–X	19.44, 20.13
		(V_1–C_{26})	W–L–Γ	20.72
		(V_3–C_{25})	W–L–Γ–X–W–K	19.69, 20.36
		(V_3–C_{26})	W–L–Γ	21.07
		(V_4–C_{24})	L–Γ–X	19.94
		(V_4–C_{25})	W–L–Γ–X–W	19.69, 20.34
		(V_4–C_{26})	W–L–Γ	21.07
		(V_5–C_{24})	L–Γ–X	19.82
		(V_5–C_{25})	W–L–Γ–X	19.75, 20.61
		(V_5–C_{26})	W–L–Γ	20.95

attain a maximum value; then, they decrease for higher energy values. The static refractive index $n(0)$ values for $SiMg_2O_4$, $SiZn_2O_4$ and $SiCd_2O_4$ and the energy when dispersion is null $E(n=1)$ are shown in Table 4. The static refractive index $n(0)$ value increases from $SiMg_2O_4$ to $SiCd_2O_4$, which follows an opposite trend from the band gap (the band gap decreases from $SiMg_2O_4$ to $SiCd_2O_4$). The refractive index attains a maximum value of 2.030, 2.089 and 2.087 at 11.52, 10.24 and 8.97 eV for $SiMg_2O_4$, $SiZn_2O_4$ and $SiCd_2O_4$, respectively. The pressure derivative of the static refractive index $n(0)$ of these compounds is determined using a linear fit, and the results are listed in Table 4. As shown in this table, an increase in pressure leads to a decrease in the refractive index.

The absorption coefficient reveals the radiation absorbing mechanism of the medium. Fig. 7 displays the absorption coefficient $\alpha(\omega)$ of the three considered compounds as a function of the photon energy. The $SiMg_2O_4$ compound ($SiZn_2O_4$ and $SiCd_2O_4$) has an absorption band from approximately 7.5 to 28 eV (5.5–28 eV and 3.5–28 eV, respectively), which reaches its maximum at approximately 20.8 eV (at approximately 16.5 eV and 17.8 eV, respectively). These materials are transparent in the visible region and absorptive in the ultraviolet region. In the high-energy region (above 28 eV), these compounds are transparent because it becomes progressively more difficult for the electrons to respond.

Table 6
Peak positions of $\varepsilon_2(\omega)$ with the dominant interband transition contributions to every peak and their location in the Brillouin zone for $SiZn_2O_4$.

Optical structures		Dominant interband transition contributions		
Structure	Peak position	Transition	Region	Energy (eV)
E_0	4.70	(V_1–C_1)	Γ–Γ	
E_1	8.15	(V_1–C_1)	W–L, Γ–X	7.51, 7.68
		(V_1–C_2)	W–L, Γ–X–W–K	7.95, 8.10, 8.16
		(V_1–C_3)	W–L–Γ–X, W–K	9.62
		(V_2–C_1)	L–Γ–X	7.18
		(V_2–C_2)	W–L–Γ–X–W–K	7.76, 8.33
		(V_2–C_3)	W–L–Γ–X, W–K	9.73
		(V_3–C_1)	W–L–Γ–X	7.47, 8.35
		(V_3–C_2)	W–L, X–W–K	8.58
		(V_4–C_1)	W–L–Γ–X	7.72, 7.84
		(V_4–C_2)	W–L–Γ–X–W–K	8.03, 8.76
		(V_5–C_1)	L–Γ–X	7.72
		(V_5–C_2)	W–L–Γ–X–W–K	8.05, 8.91
E_2	10.60	(V_{11}–C_1)	L–Γ–X	9.18
		(V_{13}–C_1)	L–Γ–X	9.54
		(V_{14}–C_1)	L–Γ–X	9.41, 10.62
		(V_{15}–C_1)	L–Γ–X	8.97, 10.60
		(V_{15}–C_2)	W–L–Γ–X	11.04
		(V_{16}–C_1)	W–L–Γ–X	10.21, 10.80
		(V_{16}–C_2)	W–L, Γ–X	11.08
		(V_{17}–C_1)	W–L–Γ–X	10.45, 10.64
E_3	11.20	(V_{11}–C_1)	W–L, Γ–X	11.42, 11.79
		(V_{11}–C_2)	W–L–Γ–X–W–K	11.65,11.92
		(V_{12}–C_1)	W–L–Γ–X	11.27, 11.54
		(V_{13}–C_1)	W–L, Γ–X	11.46
		(V_{13}–C_2)	W–L, Γ–X–W–K	11.29, 11.84
		(V_{14}–C_1)	W–L, Γ–X	11.63
		(V_{14}–C_2)	W–L, Γ–X	11.27, 11.56
		(V_{15}–C_2)	W–L, Γ–X, W–K	11.69
		(V_{15}–C_5)	L–Γ–X	11.88
		(V_{16}–C_2)	W–L, Γ–X, W–K	11.50, 11.67
		(V_{17}–C_1)	W–L, Γ–X	11.24
		(V_{17}–C_2)	W–L	11.46
		(V_{18}–C_1)	W–L, Γ–X	11.23
		(V_{18}–C_2)	W–L, Γ–X–W	11.36
E_4	12.69	(V_{13}–C_3)	L–Γ–X	12.50
		(V_{13}–C_4)	L–Γ–X	12.42
		(V_{13}–C_5)	L–Γ–X	12.19
		(V_{14}–C_3)	L–Γ–X	12.21
		(V_{14}–C_4)	L–Γ–X	12.30
		(V_{14}–C_5)	L–Γ–X	12.17
E_5	13.33	(V_{13}–C_3)	W–L–Γ–X, W–K	13.19
		(V_{13}–C_4)	W–L–Γ–X–W–K	13.51
		(V_{13}–C_5)	L–Γ–X	13.82
		(V_{14}–C_3)	L–Γ–X, W–K	13.01
		(V_{14}–C_4)	W–L–Γ–X–W–K	13.51
		(V_{15}–C_4)	W–L–Γ–X–W–K	13.55
		(V_{15}–C_5)	W–L, Γ–X–W	13.74, 13.99
		(V_{15}–C_6)	W–L–Γ	13.78
		(V_{16}–C_4)	W–L, Γ–X	13.44
		(V_{16}–C_5)	L–Γ–X	13.38, 13.61
E_6	15.22	(V_{11}–C_9)	W–L–Γ	14.93
		(V_{11}–C_{10})	L–Γ–X	16.01
		(V_{12}–C_8)	Γ–X–W	14.49
		(V_{12}–C_9)	W–L–Γ	15.20
		(V_{12}–C_{10})	W–L–Γ–X	16.01
		(V_{13}–C_8)	W–L, Γ–X–W	14.49, 14.93
		(V_{13}–C_9)	W–L–Γ, X–W–K	15.18, 15.51
		(V_{14}–C_9)	W–L–Γ	15.28
		(V_{15}–C_8)	W–L, Γ–X	14.74
		(V_{15}–C_9)	W–L–Γ	15.39
		(V_{16}–C_8)	W–L, Γ–X	14.74
		(V_{16}–C_9)	L–Γ–X	15.64
E_7	16.27	(V_{13}–C_{10})	W–L, Γ–X	16.33
		(V_{13}–C_{11})	W–L–Γ, X–W	16.56
		(V_{14}–C_{10})	W–L–Γ–X	16.20
		(V_{14}–C_{11})	W–L	16.33
		(V_{15}–C_{10})	W–L, Γ–X	16.10
		(V_{15}–C_{11})	W–L–Γ, X–W–K	16.33
		(V_{15}–C_{12})	L–Γ–X–W–K	17.02
		(V_{16}–C_{10})	L–Γ–X	16.10
		(V_{16}–C_{11})	W–L–Γ, X–W	17.36, 16.79

Table 7
Peak positions of $\varepsilon_2(\omega)$ with the dominant interband transition contributions to every peak and their location in the Brillouin zone for $SiCd_2O_4$.

Optical structures		Dominant interband transition contributions		
Structure	Peak position	Transition	Region	Energy (eV)
E_0	3.43	(V_1–C_1)	Γ–Γ	
E_1	6.068	(V_3–C_1)	W–L–Γ–X	5.80
		(V_3–C_2)	W–L, X–W–K	6.51
		(V_4–C_1)	W–L, Γ–X	5.92
		(V_4–C_2)	W–L, X–W–K	6.51
		(V_5–C_1)	L–Γ–X	5.80
		(V_5–C_2)	W–L, Γ–X–W–K	6.74
		(V_{13}–C_1)	L–Γ–X	6.40
		(V_{14}–C_1)	Γ–X–W	5.80
E_2	7.73	(V_3–C_3)	W–L–Γ–X	8.43
		(V_4–C_3)	W–L–Γ–X, W–K	8.58
		(V_5–C_3)	W–L–Γ–X	8.70
		(V_{13}–C_1)	W–L, Γ–X	7.72
		(V_{13}–C_2)	W–L–Γ–X–W–K	7.41, 8.12
		(V_{14}–C_1)	W–L, Γ–X	8.03
		(V_{14}–C_2)	W–L–Γ–X–W–K	7.24, 8.26
E_3	9.25	(V_3–C_4)	W–L–Γ–X–W–K	9.04
		(V_3–C_5)	W–L, Γ–X	9.29, 9.77
		(V_3–C_6)	L–Γ–X	9.50
		(V_4–C_4)	W–L, Γ–X–W–K	9.10
		(V_4–C_5)	W–L, X–W	9.83
		(V_4–C_6)	L–Γ–X–W	9.98
		(V_5–C_4)	W–L, Γ–X–W–K	9.27
		(V_{13}–C_3)	L–Γ–X	9.29
		(V_{13}–C_4)	L–Γ–X	9.66
		(V_{14}–C_3)	L–Γ–X	8.87, 9.18
		(V_{14}–C_5)	L–Γ–X	8.93
E_4	10.99	(V_4–C_7)	W–L–Γ–X	10.73, 11.10
		(V_4–C_8)	L–Γ–X	11.02
		(V_5–C_5)	W–L, X–W	10.31
		(V_5–C_6)	L–Γ–X	10.21
		(V_5–C_7)	L–Γ–X	10.94
		(V_5–C_8)	L–Γ–X	10.62
		(V_{13}–C_3)	W–L–Γ–X, W–K	10.12
		(V_{13}–C_4)	W–L–Γ–X–W–K	10.62
		(V_{13}–C_5)	W–L, Γ–X	10.92
		(V_{14}–C_3)	W–L–Γ–X, W–K	10.12
		(V_{14}–C_4)	Γ–X–W–K	10.90
		(V_{14}–C_5)	W–L, Γ–X–W	11.71
		(V_{25}–C_1)	L–Γ–X	11.00
		(V_{25}–C_2)	W–L–Γ–X	11.46
E_5	12.89	(V_4–C_9)	W–L–Γ, W–K	12.07
		(V_4–C_{10})	W–L, X–W–K	12.27
		(V_4–C_{11})	L–Γ–X–W	12.90
		(V_4–C_{12})	W–L, X–W–K	12.71, 12.96
		(V_5–C_9)	W–L–Γ–X–W	12.00, 12.48
		(V_5–C_{10})	W–L–Γ, X–W–K	12.50
		(V_5–C_{11})	W–L–Γ	12.84
		(V_5–C_{12})	W–L–Γ, X–W–K	12.96
		(V_{13}–C_6)	L–Γ, X–W–K	11.84, 12.63
		(V_{13}–C_7)	W–L–Γ–X	11.81, 12.65
		(V_{14}–C_7)	L–Γ–X	12.04
E_6	13.69	(V_4–C_{13})	W–L–Γ–X, W–K	13.67
		(V_4–C_{14})	W–L, Γ–X	13.74
		(V_4–C_{15})	W–L, Γ–X, W–K	14.24

Table 7 (*continued*)

Optical structures		Dominant interband transition contributions		
Structure	Peak position	Transition	Region	Energy (eV)
		(V_5–C_{13})	W–L, Γ–X, W–K	13.70, 13.86
		(V_5–C_{14})	W–L, Γ–X, W–K	13.86, 14.16
		(V_5–C_{15})	W–L, Γ–X	14.41
		(V_{13}–C_7)	Γ–X–W	13.49
		(V_{13}–C_8)	Γ–X–W–K	13.15, 13.57
		(V_{13}–C_9)	W–L, Γ–X, W–K	13.49
		(V_{14}–C_7)	W–L, Γ–X–W	13.00, 13,57
		(V_{14}–C_8)	Γ–X–W–K	13.26, 13.61
		(V_{14}–C_9)	W–L, Γ–X, W–K	13.67
		(V_{14}–C_{10})	Γ–X	13.67
		(V_{24}–C_5)	L–Γ–X	13.90
E_7	15.47	(V_4–C_{18})	L–Γ	15.41
		(V_4–C_{19})	W–L–Γ–X	15.28
		(V_4–C_{20})	W–L, Γ–X, W–K	15.28
		(V_4–C_{21})	W–L–Γ–X–W–K	15.43, 15.85
		(V_5–C_{17})	W–L–Γ–X	14.89, 15.26
		(V_5–C_{18})	L–Γ–X	14.70, 15.41
		(V_5–C_{19})	W–L–Γ–X–W–K	15.41
		(V_5–C_{20})	L–Γ–X–W	15.43
		(V_{14}–C_{13})	W–L–Γ–X, W–K	15.41
		(V_{14}–C_{14})	L–Γ–X	15.41
		(V_{14}–C_{15})	L–Γ–X	15.41
E_8	15.79	(V_4–C_{22})	W–L–Γ–X–W–K	16.10
		(V_4–C_{23})	W–L, Γ–X, W–K	16.33
		(V_5–C_{21})	L–Γ–X–W	15.62
		(V_5–C_{22})	W–L–Γ–X–W–K	16.20
		(V_5–C_{23})	L–Γ	16.41
		(V_{14}–C_{15})	W–L, Γ–X, W–K	15.87
		(V_{14}–C_{16})	L–Γ–X	16.20
		(V_{14}–C_{17})	L–Γ–X	16.10
E_9	17.38	(V_4–C_{23})	W–L, Γ–X	17.00, 17,16
		(V_4–C_{24})	W–L, Γ–X	17.37
		(V_5–C_{23})	W–L, Γ–X	17.44
		(V_{13}–C_{22})	W–L, Γ–X–W–K	17.60
		(V_{13}–C_{23})	Γ–X–W–K	17.69, 18.06
		(V_{14}–C_{19})	W–L–Γ	17.02
		(V_{14}–C_{21})	L–Γ, X–W–K	17.48
		(V_{14}–C_{22})	W–L, Γ–X–W–K	17.71
		(V_{14}–C_{23})	Γ–X, W–K	17.96

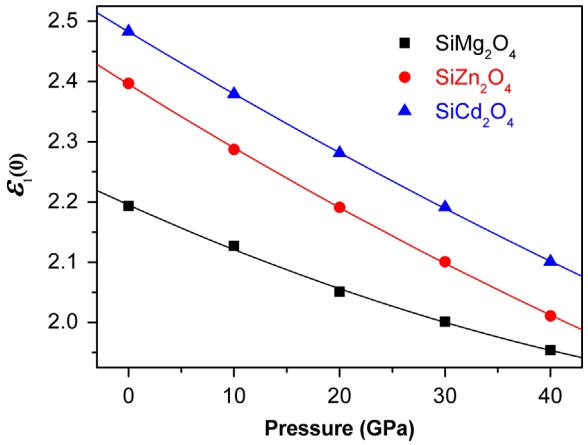

Fig. 5. Pressure dependence of the static dielectric constant $\varepsilon(0)$ of the spinel oxides $SiMg_2O_4$, $SiZn_2O_4$ and $SiCd_2O_4$.

In Fig. 8, we show the calculated reflectivity spectrum $R(\omega)$ and the electron energy loss spectra $L(\omega)$ for the $SiMg_2O_4$, $SiZn_2O_4$ and $SiCd_2O_4$ compounds. The reflectivity $R(\omega)$ values begin to increase from a relatively small value (3.74% for $SiMg_2O_4$, 4.63% for $SiZn_2O_4$, and 4.98% for $SiCd_2O_4$) to attain a maximum value (62.25% for photon energy at approximately 22.92 eV for $SiMg_2O_4$, 62.97% at

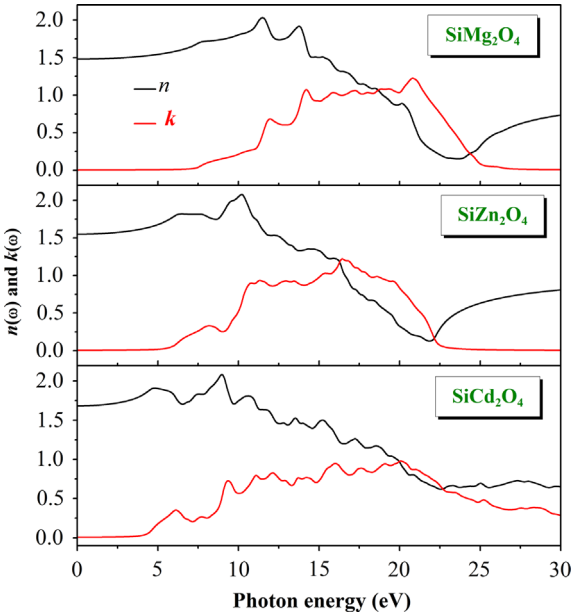

Fig. 6. Refractive index $n(\omega)$ and extinction coefficient $k(\omega)$ of the spinel oxides $SiMg_2O_4$, $SiZn_2O_4$ and $SiCd_2O_4$ as calculated using the TB-mBJ functional.

21.84 eV for $SiZn_2O_4$, and 41.14% at 20.38 eV for $SiCd_2O_4$). Then, the reflectivity quickly decreases for higher energy values. The electron energy loss function $L(\omega)$ is an important optical factor that describes the energy loss of a fast traversing electron in a material. The peaks in the $L(\omega)$ spectrum are interpreted as Plasmon peaks, which denote the electronic charge collective oscillations in the crystal, and the corresponding frequencies are the so-called plasma frequencies. The peaks of $L(\omega)$ overlap the trailing edges in the reflection spectra. For instance, the peaks of the $L(\omega)$ spectra for $SnMg_2O_4$, $SnZn_2O_4$ and $SnCd_2O_4$ are at approximately 24.5, 22.2 and 21.8 eV, respectively, which correspond to the abrupt reduction of $R(\omega)$.

4. Conclusions

We have used an ab initio FP-L/APW+lo method to explore the structural, electronic and optical properties of the spinel oxides $SnMg_2O_4$, $SnZn_2O_4$ and $SnCd_2O_4$. The computed structural parameters are consistent with the available experimental findings and previous theoretical results, which validates the method that we used. We investigated the electronic properties using four different functionals: LDA, GGA-PBEsol, GGA-EV and TB-mBJ. We found that the TB-mBJ functional improved these properties the most. We found that these spinel oxides were direct band gap insulators with VBMa and CBMi at the Γ point. The fundamental energy band gaps of all of the considered compounds increase with increasing pressure and fit well to a quadratic function. The bottommost of the CB is dispersive, whereas the topmost of the VB is dispersionless, which predicts a higher hole effective mass. Consequently, the mobility of the VB holes in these materials should be small. The fundamental band gap decreases from $SiMg_2O_4$ to $SiZn_2O_4$ to $SiCd_2O_4$. The dielectric function and the optical parameters, such as the refractive index, extinction coefficient, absorption coefficient, reflectivity and electron energy loss function, were predicted for a wide range between 0 and 30 eV. The decomposition of the dielectric functions into individual band-to-band contributions and the plotting of the transition band structures allowed us to identify the microscopic origin of the features in the optical spectra and the contributions of different regions in the Brillouin

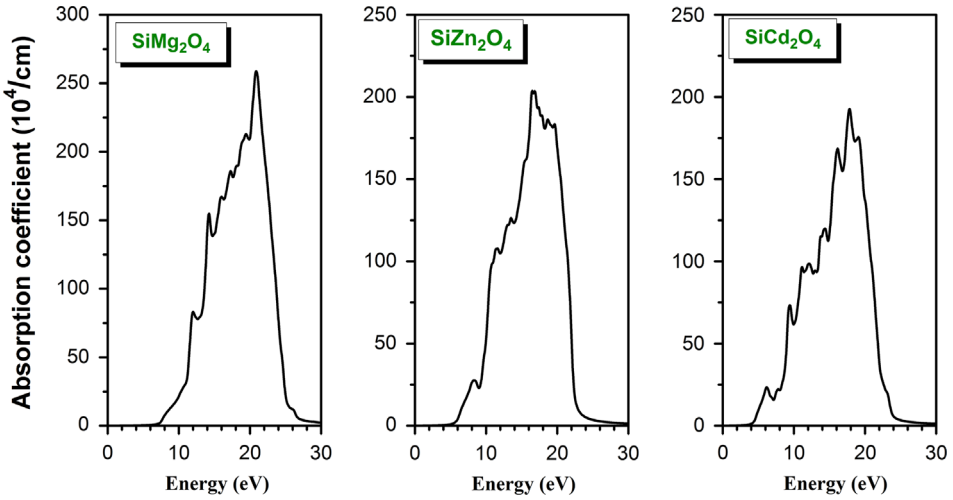

Fig. 7. Absorption spectra of the spinel oxides $SiMg_2O_4$, $SiZn_2O_4$ and $SiCd_2O_4$ as calculated using the TB-mBJ functional.

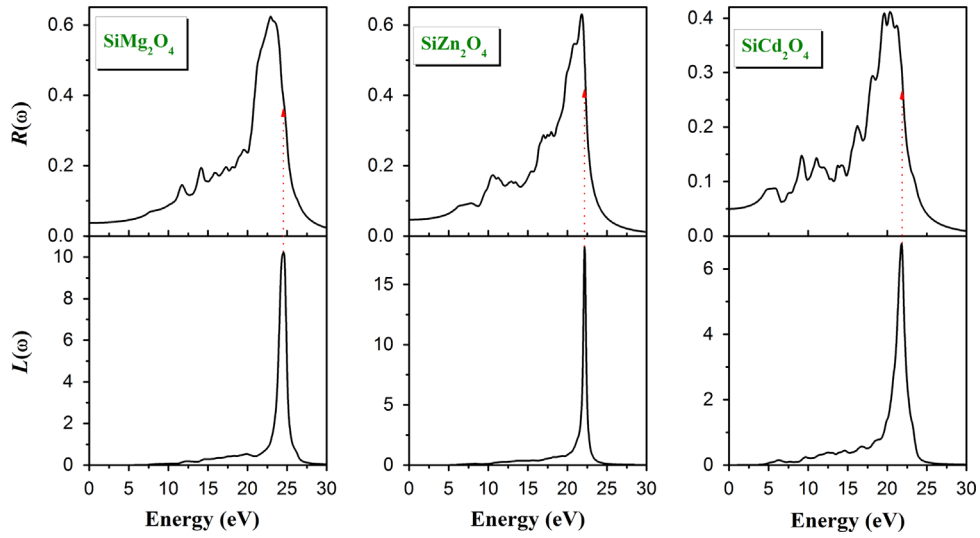

Fig. 8. Reflectivity spectrum $R(\omega)$ and electron energy loss function $L(\omega)$ for the spinel oxides $SiMg_2O_4$, $SiZn_2O_4$ and $SiCd_2O_4$ as calculated using the TB-mBJ functional.

zone. We found that the values of $\varepsilon_1(0)$ increased when the energy gap decreased, which could be explained using the Penn model.

Acknowledgment

Bin-Omran acknowledges the support by the National Plan for Science, Technology and Innovation under the research Project no. NANO-673-2. The authors extend their appreciation to the Deanship of Scientific Research at King Saud University for funding the work through research group Project no. RGP-VPP-088. For the author A.H. Reshak the result was developed within the CENTEM project, reg. no. CZ.1.05/2.1.00/03.0088, co-funded by the ERDF as part of the Ministry of Education, Youth and Sports OP RDI programme.

References

[1] T. Sonehara, K. Kato, K. Ozaka, M. Takata, T. Katsufuji, Phys. Rev. B 74 (2006) 104424.
[2] U.O. Okeke, J.E. Lowther, Phys. Rev. B 77 (2008) 094129.
[3] K. Nomura, H. Ohta, T. Ueda, M. Hirano, H. Hosono, Science 300 (2003) 1269.
[4] B.G. Lewis, D.C. Paine, MRS Bull. 25 (2000) 22.
[5] D. Segev, S.H. Wei, Phys. Rev. B 71 (2005) 12529.
[6] S.H. Wei, S.B. Zhang, Phys. Rev. B 63 (2001) 045112.
[7] R. Nistora, A.S. Gruia, Optoelectron. Adv. Mater. 6 (2012) 717.
[8] A. Bouhemadou, R. Khenata, F. Zerarga, Eur. Phys. J. B 56 (2007) 1.
[9] X. Shen, J. Shen, S.J. You, L.X. Yang, L.Y. Tang, Y.C. Li, J. Liu, H. Hang, K. Zhu, Y.L. Liu, W.Y. Zhou, C.Q. Jin, R.C. Yu, S.S. Xie, Phys. Rev. B 106 (2009) 113523.
[10] S.D. Mo, W.Y. Ching, Phys. Rev. B 54 (1996) 16555.
[11] R. Khenata, M. Sahnoun, H. Baltache, M. Rérat, Ali H. Reshak, Y. Al-Douri, B. Bouhafs, Phys. Lett. A 344 (2005) 271.
[12] L. Gracia, A. Beltrán, J. Andrés, J. Phys. Chem. C 115 (2011) 7740.
[13] Y.N. Xu, W.Y. Ching, Phys. Rev. B 43 (1991) 4461.
[14] A. Bouhemadou, R. Khenata, F. Zerarga, Comput. Mater. Sci. 39 (2007) 709.
[15] S.K. Sampath, D.G. Kambere, R. Pandey, J. Phys.: Condens. Matter 11 (1999) 3635.A.
[16] S. López, A.H. Romeo, P. Rodríguez-Hernández, A. Muñoz, Phys. Rev. B 79 (2009) 214103.
[17] A. Seko, K. Yuge, F. Oba, A. Kuwabara, I. Tanaka, Phys. Rev. B 73 (2006) 184117.
[18] L. Zhang, G.F. Ji, F. Zhao, Z.Z. Gong, Chin. Phys. B. 4 (2011) 07102.
[19] A.M. Pandàs, A. Costales, M.A. Blanco, J.M. Recio, V. Luaña, Phys. Rev. B 21 (2000) 13970.
[20] C. Aksel, B. Rand, F.L. Riley, P.D. Warren, J. Eur. Ceram. Soc. 22 (2002) 745.
[21] P. Thibaudeau, F. Gervais, J. Phys.: Condens. Matter 14 (2002) 3543.
[22] A. Bouhemadou, R. Khenata, Phys. Lett. A 360 (2006) 339.
[23] A. Ibarra, R. Vila, F.A. Garner, J. Nucl. Mater. 233 (1996) 1336.
[24] T. Suzuki, G.S. Murugan, Y. Ohishi, J. Lumin. 113 (2005) 265.
[25] J.M. Leger, J. Haines, M. Schmidt, J.P. Petitet, A.S. Pereira, J.A.H. da Jornada, Nature 383 (1996) 401.
[26] R. Pandey, J.D. Gale, S.K. Sampath, J.M. Recio, J. Am. Ceram. Soc. 82 (1999) 3337.
[27] S.K. Sampath, J.F. Cordaro, J. Am. Ceram. Soc. 81 (1998) 649.

[28] Q. Zeng, L. Zhang, X. Zhang, Q. Chen, Z. Feng, Y. Cai, L. Cheng, Z. Weng, Phys. Lett. A375 (2011) 3521.
[29] S. Soliman, A. Elfalaky, G.H. Fecher, C. Felser, Phys. Rev. B 83 (2011) 085205.
[30] L. Zhang, G.F. Ji, F. Zhao, C.M. Meng, D.Q. Wei, Physica B 406 (2011) 335.
[31] M.V. Nikolić, T. Ivetić, D.L. Young, K.M. Paraskevopoulos, T.T. Zorba, V. Blagojević, P.M. Nikolić, D. Vasiljević-Radović, M.M. Ristić, Mater. Sci. Eng. B 138 (2007) 7.
[32] G.A. de Wijs, C.M. Fang, G. Kresse, G. de With, Phys. Rev. B 65 (2002) 094305.
[33] D. Errandonea, R.S. Kumar, F.J. Manjón, V.V. Ursaki, E.V. Rusu, Phys. Rev. B 79 (2009) 024103.
[34] M. Lazzeri, P. Thibaudeau, Phys. Rev. B 74 (2006) 140301.
[35] K. Izumi, S. Miyazaki, S. Yoshida, T. Mizokawa, E. Hanamura, Phys. Rev. B 76 (2007) 075111.
[36] H. Dixit, N. Tandon, S. Cottenier, R. Saniz, D. Lamoen, B. Partoens, V Van Speybroeck, M. Waroquier, New J. Phys. 13 (2011) 063002.
[37] A. Bouhemadou, R. Khenata, Model. Simul. Mater. Sci. Eng. 15 (2007) 787.
[38] J. Łażewski, P.T. Jochym, K. Parlinski, P. Piekarz, J. Mol. Struct. 596 (2001) 3.
[39] P. Hohenberg, W. Kohn, Phys. Rev. B 136 (1964) 684.
[40] W. Kohn, L.J. Sham, Phys. Rev. A 140 (1965) 1133.
[41] W.G. Aulbur, L. Jönsson, J.W. Wilkins, Solid State Phys. 54 (2000) 1.
[42] S. Zh. Karazhanov, P. Ravindran, H. Fjellvag, B.G. Svensson, J. Appl. Phys. 106 (2009) 123701.
[43] D. Koller, F. Tran, P. Blaha, Phys. Rev. B 83 (2011) 195134.
[44] A.D. Becke, E.R. Johnson, J. Chem. Phys. 124 (2006) 221101.
[45] F. Tran, P. Blaha, Phys. Rev. Lett. 102 (2009) 226401.
[46] F. Tran, P. Blaha, K. Schwarz, J. Phys.: Condens. Matter 19 (2007) 196208.
[47] P. Blaha, K. Schwarz, G.K.H. Madsen, D. Kvasnicka, J. Luitz, WIEN2k: An Augmented Plane wave+Local Orbitals Program for calculating Crystal Properties, Wien, Austria, Karlheinz Schwarz, Techn. Universität, 2011, ISBN: 3-950131-1-2.
[48] H. Dixit, R. Saniz, S. Cottenier, D. Lamoen, B. Partoens, J. Phys.: Condens. Matter 24 (2012) 205503.
[49] J.P. Perdew, Y. Wang, Phys. Rev. B 45 (1992) 13244.
[50] J.P. Perdew, A. Ruzsinszky, G.I. Csonka, O.A. Vydrov, G.E. Scuseria, L.A. Constantin, X. Zhou, K. Burke, Phys. Rev. Lett. 100 (2008) 136406.
[51] E. Engel, S.H. Vosko, Phys. Rev. B 47 (1993) 13164.
[52] H.J. Monkhorst, J.D. Pack, Phys. Rev. B 13 (1976) 5188.
[53] J.A. Camargo-Martínez, R. Baquero, Phys. Rev. B 86 (2012) 195106.
[54] P. Dufek, P. Blaha, K. Schwarz, Phys. Rev. B 50 (1994) 7279.
[55] S. Zh. Karazhanov, P. Ravindran, H. Fjellvag, B.G. Svensson, J. Appl. Phys. 106 (2009) 123701.
[56] S.H. Wei, A. Zunger, Phys. Rev. B 37 (1988) 8958.
[57] A. Bouhemadou, Model. Simul. Mater. Sci. Eng. 16 (2008) 055007.
[58] W.R.L. Lambrecht, A.V. Rodina, S. Limpijumnong, B. Segal, B.K. Meyer, Phys. Rev. B 65 (2002) n075207.
[59] K. Hümmer, Phys. Status Solidi B 56 (1973) 249.
[60] D. Allali, A. Bouhemadou, S. Bin-Omran, Comput. Mater. Sci. 51 (2012) 194.
[61] C. Ambrosch-Draxl, J.O. Sofo, Comput. Phys. Commun. 175 (2004) 1.
[62] D.R. Penn, Phys. Rev. 128 (1960) 2093.
[63] A.H. Reshak, Z. Charifi, H. Baaziz, Eur. Phys. J. B 60 (2007) 463.